Piezoelectric modulation of nonlinear optical response in $BaTiO_3$ thin film

Kristy J. Kormondy, Yujin Cho, Agham B. Posadas, Lu Zheng, Keji Lai, Qingxiao Wang, Moon J. Kim, Qian He, Albina Y. Borisevich, Michael C. Downer, and Alexander A. Demkov

Citation: Appl. Phys. Lett. **113**, 132902 (2018); doi: 10.1063/1.5045460
View online: https://doi.org/10.1063/1.5045460
View Table of Contents: http://aip.scitation.org/toc/apl/113/13
Published by the American Institute of Physics

Piezoelectric modulation of nonlinear optical response in $BaTiO_3$ thin film

Kristy J. Kormondy,[1] Yujin Cho,[1] Agham B. Posadas,[1] Lu Zheng,[1] Keji Lai,[1] Qingxiao Wang,[2] Moon J. Kim,[2] Qian He,[3,a)] Albina Y. Borisevich,[3] Michael C. Downer,[1] and Alexander A. Demkov[1,b)]

[1]*Department of Physics, The University of Texas at Austin, Austin, Texas 78712, USA*
[2]*Department of Materials Science and Engineering, University of Texas at Dallas, Richardson, Texas 75080, USA*
[3]*The Center for Nanophase Materials Sciences, Oak Ridge National Laboratory, Oak Ridge, Tennessee 37831, USA*

(Received 20 June 2018; accepted 11 August 2018; published online 24 September 2018)

We study the nonlinear optical response in a strained thin film ferroelectric oxide $BaTiO_3$ using piezoelectric $Pb(Mg_{1/3}Nb_{2/3})O_3$-$PbTiO_3$ (001) as a variable strain substrate and La-doped $SrTiO_3$ as a conductive buffer layer. The rotation-anisotropic second harmonic intensity profile shows hysteretic modulation corresponding to the strain variation from the inverse piezoelectric response of the substrate. An enhancement of 15% is observed at 1.2 kV/cm, while a control sample shows negligible change as a function of piezovoltage. Reflection high-energy electron diffraction, x-ray photoelectron spectroscopy, and high-resolution scanning transmission electron microscopy reveal the epitaxial interface. X-ray diffraction and piezoresponse force microscopy confirm tetragonal distortion and ferroelectricity of the $BaTiO_3$ overlayer. Our results suggest a promising route to enhance the performance of nonlinear optical oxides for the development of future nano-opto-mechanical devices. *Published by AIP Publishing.* https://doi.org/10.1063/1.5045460

Due to large lattice and thermal mismatches, one of the major problems in the fabrication of highly efficient hybrid nanophotonic modulators[1] is the diminished electro-optic coefficients of thin films.[2] When a thin oxide film is deposited heteroepitaxially, lattice mismatch and thermal mismatch can influence the film microstructure.[3] Since the linear electro-optic response stems from the loss of inversion symmetry, microstructural defects which affect phonons can diminish the electro-optic coefficients.[2] Epitaxial strain can also impact the magnitude and direction of ferroelectric polarization,[4] which in turn can impact the electro-optic response.

Owing to its large bulk electro-optic coefficients[5] and unique epitaxial integration success on Si,[3] $BaTiO_3$ (BTO) is considered a particularly promising candidate for the development of a hybrid silicon nanophotonic platform.[6] Recent studies by our group and others have shown that, compared to other thin films grown on Si,[7] BTO shows higher electro-optic coefficients and lower propagation losses.[1,2,6,8–10] It is speculated that the orientation of ferroelectric domains in particular can strongly influence the active device performance.[11] Although the electro-optic performance of BTO thin films on Si has been studied in great detail, very little has been reported on the issue of epitaxial strain. In particular, there is no information about the influence of strain on the nonlinear optical properties of BTO. Such an understanding can be obtained by studying nonlinear optical properties under varying epitaxial strains and is of key importance in approaching the overarching goal of efficient hybrid oxide nanophotonics.

In this paper, we performed such a study on the nonlinear optical response in BTO using piezoelectric single crystal $Pb(Mg_{1/3}Nb_{2/3})O_3$-$PbTiO_3$ (PMN-PT) (001) as a variable strain substrate and La-doped $SrTiO_3$ (LSTO) as a conductive buffer layer. The rotation-anisotropic second harmonic intensity profile shows hysteretic modulation corresponding to the strain variation from the inverse piezoelectric response of the substrate. An enhancement of 15% is observed at an applied electric field of 1.2 kV/cm, while a control sample with no BTO shows a negligible change as a function of piezovoltage. Reflection high-energy electron diffraction (RHEED), x-ray photoelectron spectroscopy (XPS), and high-resolution scanning transmission electron microscopy (STEM) reveal the excellent crystalline quality of the different layers and their interfaces. X-ray diffraction (XRD) and piezoresponse force microscopy (PFM) in the spectroscopy mode[12] confirm tetragonal distortion and ferroelectricity of the BTO overlayer. Our results suggest a promising route to enhance the performance of nonlinear optical oxides for the development of future nano-opto-mechanical devices.

The oxide heterostructures were grown using molecular beam epitaxy (MBE). PMN-PT substrates with dimensions $5 \times 5 \times 0.5\,mm^3$ were ultrasonically cleaned for 5 min each with acetone, isopropanol, and deionized water, followed by 15 min of exposure to UV/ozone. After a 10 min outgassing in vacuum at 600 °C, the oxide films were deposited on the substrate using a customized DCA Instruments oxide MBE system with a base pressure of 8.0×10^{-10} Torr. La, Sr, Ba, and Ti metal sources were heated in individual effusion cells for shuttered deposition at a total growth rate equivalent to ~2 Å/min calibrated using a quartz crystal microbalance. Molecular oxygen was provided at a partial pressure of 5×10^{-6} Torr during film deposition for both BTO and LSTO. *In situ* reflection high-energy electron diffraction (RHEED) oscillations served as a second check of the thin-film deposition rate [see supplementary material, Fig. S1(a)].

a)Permanent address: School of Chemistry, Cardiff University, Cardiff, UK.
b)demkov@physics.utexas.edu

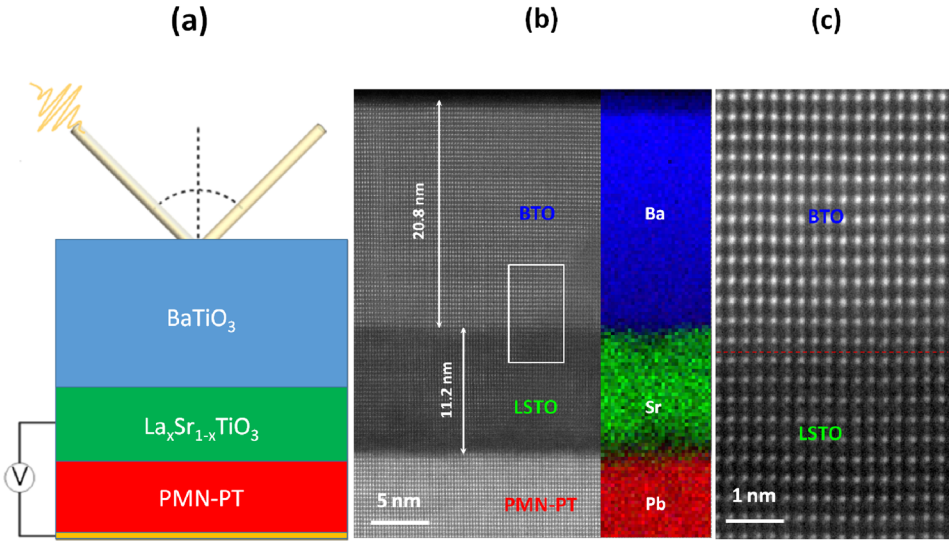

FIG. 1. (a) Overall schematic, including the silver paste as a bottom electrode (yellow), bulk PMN-PT substrate (red), layer of STO with x% La replacing Sr (green), and BTO film (blue), not to scale. (b) High resolution HAADF image of the BTO/LSTO/PMN-PT interface along the [100]-projection of the PMN-PT substrate. False color EDS mapping has been overlaid on the HAADF image, showing the distribution of Ba (blue), Sr (green), and Pb (red), respectively. (c) Magnified BTO/LSTO surface from the highlighted (white rectangle) region in (b), showing the perfect lattice match between BTO and LSTO.

The film composition is checked using x-ray photoelectron spectroscopy (XPS) after the growth of each layer [see supplementary material, Fig. S1(b)].

A schematic diagram of the heterostructure is shown in Fig. 1(a) including the bulk PMN-PT substrate (red), buffer layer of conductive LSTO with 15% La replacing Sr (green), BTO film (blue), and silver paste as a bottom electrode (yellow). Depending on the bias voltage applied across the PMN-PT, the inverse piezoresponse can change the epitaxial strain imposed on the BTO layer, as demonstrated in Refs. 13–15. The details of the LSTO and BTO thin film deposition can be found in our recent publications.[16,17]

High resolution high angle annular dark field (HAADF)-STEM imaging is conducted using an aberration-corrected JEM-ARM200F (JEOL USA, Inc.) operated at 200 kV in order to study the interface in more detail. The STEM specimens were prepared using a focused ion beam (FEI Nano 200 Dual Beam).[18] The convergence semi-angle is set to 24 mrad, and the collection semi-angle for the annular dark-field (ADF) detector is 90–370 mrad. Energy dispersive x-ray spectroscopy (EDS) mapping is carried out using an X-Max^N 100TLE detector (Oxford Instruments). Figure 1(b) shows a typical high-angle annular dark-field scanning transmission electron microscopy image of the interface projected along the [110] BTO zone axis. A corresponding false-color EDS mapping has been overlaid on the STEM image to show the elemental distribution of Pb (red), Sr (green), and Ba (blue), respectively. The measured thicknesses of 11 nm LSTO and 21 nm BTO are in very good agreement with the calibrated evaporation rates.

Figure 1(c) shows a zoomed-in image of the BTO/LSTO interface inside the boxed region in Fig. 1(b). The lattice of BTO perfectly matches with the LSTO buffer layer, indicating excellent epitaxy between BTO and LSTO. Although there is a 3% lattice mismatch with dislocations in some regions of LSTO from the low magnification image (not shown), TEM imaging suggests that the LSTO layer is nearly fully relaxed by the misfit dislocations, in good agreement with the XRD results. The out-of-plane and in-plane XRD results are shown in Figs. 2(a) and 2(b), which indicate the fully relaxed 0.39 nm LSTO lattice parameter. Figure 2(c)

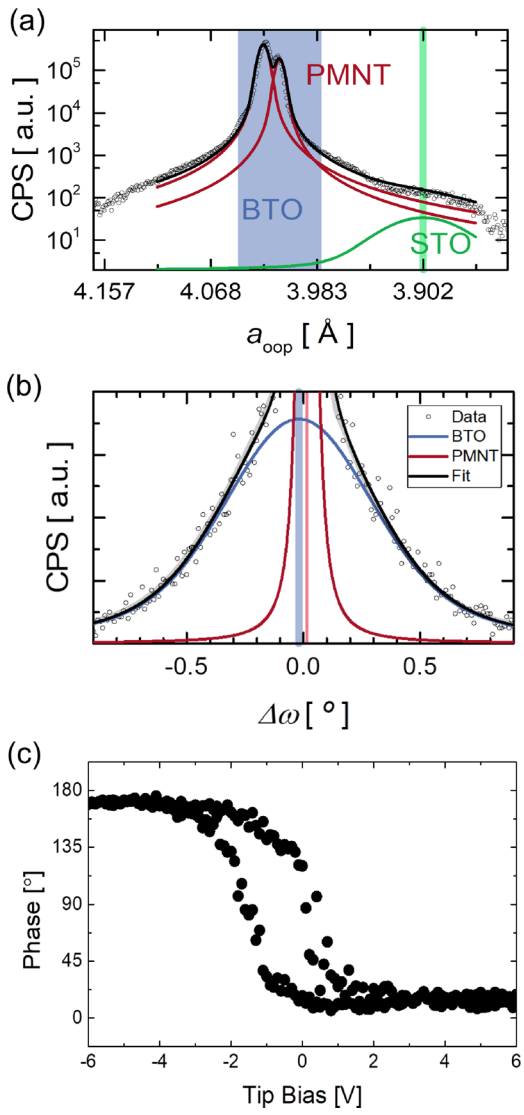

FIG. 2. (a) X-ray diffraction coupled scan of the BTO, PMN-PT, and LSTO (002) peaks. Experimental data points are shown by open circles, and a sum of two Voigt functions has been fitted to the data. The STO bulk lattice constant is indicated with a green line. (b) Rocking curve data and analysis of the (002) reflection of the 20 nm BTO film. (c) Hysteresis loops measured by PFM for the BTO film thickness of 20 nm.

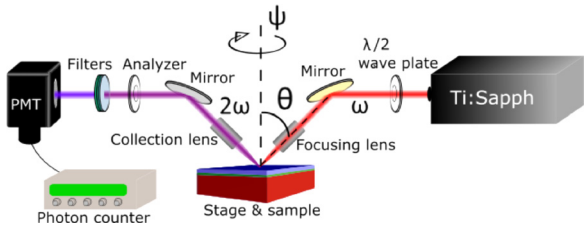

FIG. 3. Schematic of SHG diagnostics. The filter set is a composite of two color filters (BG 39) and one bandpass filter centered at 390 nm. We used a film polarizer for the analyzer and a zero-order $\lambda/2$ wave plate.

shows hysteresis loops measured by PFM for a 20 nm BTO/10 nm LSTO/PMN-PT heterostructure with the conductive LSTO layer grounded, consistent with a uniform, out-of-plane polarized BTO layer.

Optical second-harmonic generation (SHG) microscopy was used to measure the voltage-induced changes in SHG on the control (LSTO/PMN-PT) and the heterostructure (BTO/LSTO/PMN-PT) samples. Light from a Ti:Sapphire laser operated in the pulsed mode with a wavelength of 780 nm, a repetition rate of 76 MHz, and a duration of 150 fs was impinged on the sample at an angle of 45° with s-polarization, focused to a spot size of ~15 μm FWHM on the sample surface. A photomultiplier tube detected the p-polarized SHG signal in reflection through bandpass filters to suppress reflected fundamental light. To avoid electron charging or damage, we kept the laser power below 10 mW. All measurements were performed at room temperature. Figure 3 shows the SHG microscopy schematic setup.

We checked the uniformity of the samples by scanning over $100 \times 100\ \mu m^2$. SHG intensities varied within 20% across the area. On the same spot, the uncertainty from the laser fluctuation was less than 2%. SHG was measured while the sample was rotating (rotational anisotropy SHG; RASHG) to see the crystallographic orientation dependence of SHG at the applied voltage. During the azimuthal angle rotation, instead of the laser beam remaining on the same spot, it circled within 100 μm in diameter.

Figure 4(a) shows RASHG on the control sample (LSTO/PMN-PT) and the heterostructure (BTO/LSTO/PMN-PT) sample without the external electric field. The heterostructure sample showed ~20% higher SHG intensity than the control sample. PMN-PT (001) has a pseudo-cubic crystal structure, and the unit cell is distorted by 0.1° along the polarization direction.[15] RASHG of PMN-PT has four peaks due to the cubic structure, which could be described as $\sin 2\phi$. The BTO layer belongs to the C_{4v} symmetry group whose azimuthal angle dependence is isotropic in the s-in/p-out polarization configuration. In Fig. 4, RASHG on the control sample (LSTO/PMN-PT) shows variation in peak intensities. SHG intensities of the first and the third peaks are stronger than those of the second and the fourth peaks. This could arise from interfering second harmonic fields between an anisotropic bulk PMN-PT of the form $B \sin 2\phi$ and an isotropic surface or interface second harmonic field A. If the phase difference between two sources is α, the collective SHG intensity has the form

$$I_{SHG} = \left|A + B \exp(i\alpha) \sin 2\phi\right|^2, \quad (1)$$

where B is a Fresnel factor and ϕ is the azimuthal angle. This fits the experimental data well, as shown in Fig. 4(a). Asymmetry of the peak intensities increases in the heterostructure sample (BTO/LSTO/PMN-PT).

To see voltage-induced changes to SHG from the BTO film, we applied silver paint to the back of the substrate to serve as a bottom electrode. Two additional top contacts secured by silver paint ensured the Ohmic contact to the LSTO layer. The applied voltage was limited to the range ± 60 V (~1.2 kV/cm). At higher voltages, there were voltage-induced changes to the PMN-PT substrate that also affected SHG because its probe depth exceeded the film thickness. For example, at +80 V, SHG intensity in some areas increased due to the leakage current. This could be overcome by carefully controlling the oxygen vacancies or defects in the film. Around +100 V, ferroelectric domains on the PMN-PT substrate formed. At >75 V, corresponding to fields exceeding 1.5 kV/cm at room temperature, single-crystal PMN-PT substrates can be poled.[19] Lowering the fundamental wavelength or having a thicker film, but below the critical thickness, could help to isolate the SHG signal on BTO layers from the PMN-PT substrate.

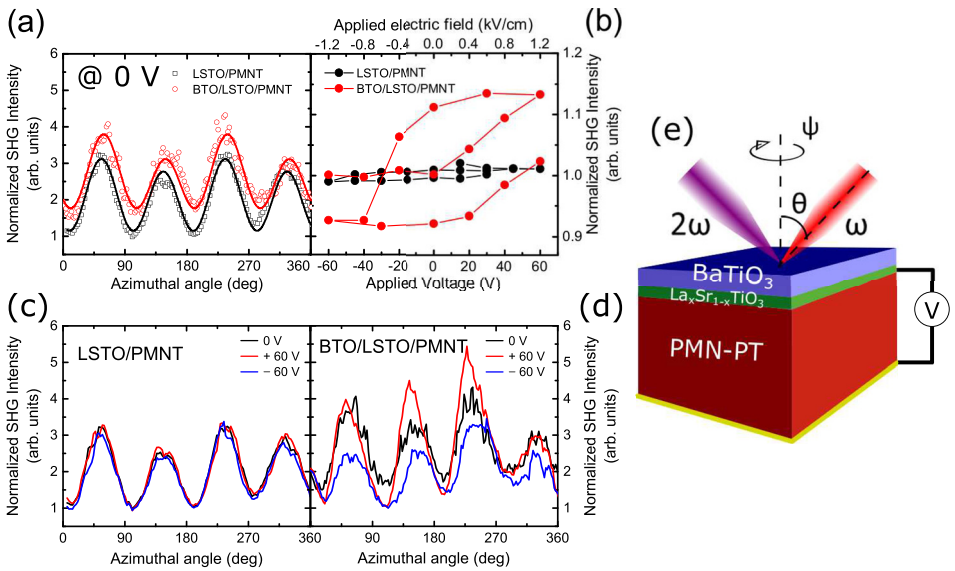

FIG. 4. (a) Rotational anisotropy SHG (RASHG) pattern on the control sample and the heterostructure without external voltage applied on the PMN-PT substrate. Open circles are experimental data, and solid lines are fitting from Eq. (1). (b) SHG intensity change at different voltages. Black (red) circles indicate SHG intensities on the control (heterostructure) sample. (c) and (d) are RASHG at 0 and ±60 V on the control sample and the heterostructure sample, respectively. (e) Schematic of the RASHG measurement with *in situ* voltage control.

As shown in Fig. 4(b), the control sample showed very little change over the voltage range, which fell within the uncertainty of SHG intensity from the laser fluctuation. The RASHG pattern [Fig. 4(c)] at ±60 V further confirmed that there is no significant change due to the external electric field. The heterostructure sample, in contrast, showed a clear SHG intensity change [Fig. 4(d)] with the applied voltage. At ±60 V, the peaks of RASHG increased/decreased by ∼15%. When the positive voltage was applied to the PMN-PT substrate, SHG intensity increased, while it decreased with the negative voltage. In addition to this, SHG intensities at 0 V maintained the same SHG intensity level as the previously applied voltage. It suggests that there was a remaining effect on the BTO overlayer. Similar hysteresis has been observed in the electrical resistance of VO_2 films on PMN-PT as the electric field cycled below the coercive field of the PMN-PT substrate.[20] XRD measurements confirmed that the hysteresis was induced by the hysteresis of the strain,[21] related to the structural rearrangement of the ferroelectric domain on the PMN-PT substrate. We therefore infer that the hysteresis loops in Figs. 4(b) and 4(d) were from the changing ferroelectric polarization of the BTO film, as modulated by the changing strain induced by the PMN-PT substrate. This variation from area to area reflects the inhomogeneous distribution of defects or impurities.

In conclusion, we explored the nonlinear optical response in BTO using piezoelectric PMN-PT (001) as a variable strain substrate and La-doped $SrTiO_3$ (LSTO) as a conductive buffer layer. Reflection high-energy electron diffraction, x-ray photoelectron spectroscopy, and high-resolution transmission electron microscopy reveal the high quality epitaxial nature of the heterostructure. X-ray diffraction and piezoresponse force microscopy confirm tetragonal distortion and ferroelectricity of the BTO overlayer. The rotation-anisotropic second harmonic intensity profile demonstrates hysteretic modulation corresponding to the strain variation from the inverse piezoelectric response of the substrate. An enhancement of the SHG signal of 15% is observed at an applied external electric field of 1.2 kV/cm, while a control sample shows negligible change as a function of piezovoltage. Our results suggest a promising route to control the performance of nonlinear optical oxides for the development of future nano-opto-mechanical devices.

See supplementary material for the details of RHEED and XPS analyses of the films.

This work was supported by the Air Force Office of Scientific Research (FA9550-12-10494 and FA9550-18-1-0053) and the Robert Welch Foundation (F-1038). L.Z. and K.L. were supported by the National Science Foundation (DMR-1707372). M.K. was supported in part by Louis Beecherl, Jr. endowment funds.

[1]S. Abel, T. Stöferle, C. Marchiori, C. Rossel, M. D. Rossell, R. Erni, D. Caimi, M. Sousa, A. Chelnokov, B. J. Offrein *et al.*, "A strong electro-optically active lead-free ferroelectric integrated on silicon," Nat. Commun. **4**, 1671 (2013).

[2]K. J. Kormondy, Y. Popoff, M. Sousa, F. Eltes, D. Caimi, M. D. Rossell, M. Fiebig, P. Hoffmann, C. Marchiori, M. Reinke *et al.*, "Microstructure and ferroelectricity of $BaTiO_3$ thin films on Si for integrated photonics," Nanotechnology **28**(7), 75706 (2017).

[3]C. Dubourdieu, J. Bruley, T. M. Arruda, A. Posadas, J. Jordan-Sweet, M. M. Frank, E. Cartier, D. J. Frank, S. V. Kalinin, A. A. Demkov *et al.*, "Switching of ferroelectric polarization in epitaxial $BaTiO_3$ films on silicon without a conducting bottom electrode," Nat. Nanotechnol. **8**(10), 748–754 (2013).

[4]K. J. Choi, M. Biegalski, Y. L. Li, A. Sharan, J. Schubert, R. Uecker, P. Reiche, Y. B. Chen, X. Q. Pan, V. Gopalan *et al.*, "Enhancement of ferroelectricity in strained $BaTiO_3$ thin films," Science **306**(5698), 1005–1009 (2004).

[5]M. Zgonik, P. Bernasconi, M. Duelli, R. Schlesser, P. Günter, M. H. Garrett, D. Rytz, Y. Zhu, and X. Wu, "Dielectric, elastic, piezoelectric, electro-optic, and elasto-optic tensors of $BaTiO_3$ crystals," Phys. Rev. B **50**(9), 5941 (1994).

[6]S. Abel, T. Stoferle, C. Marchiori, D. Caimi, L. Czornomaz, M. Stuckelberger, M. Sousa, B. J. Offrein, and J. Fompeyrine, "A hybrid barium titanate–silicon photonics platform for ultraefficient electro-optic tuning," J. Lightwave Technol. **34**(8), 1688–1693 (2016).

[7]B. W. Wessels, "Ferroelectric epitaxial thin films for integrated optics," Annu. Rev. Mater. Res. **37**(1), 659–679 (2007).

[8]K. J. Kormondy, S. Abel, F. Fallegger, Y. Popoff, P. Ponath, A. B. Posadas, M. Sousa, D. Caimi, H. Siegwart, E. Uccelli *et al.*, "Analysis of the Pockels effect in ferroelectric barium titanate thin films on Si(001)," Microelectron. Eng. **147**, 215–218 (2015).

[9]C. Xiong, W. H. P. Pernice, J. H. Ngai, J. W. Reiner, D. Kumah, F. J. Walker, C. H. Ahn, and H. X. Tang, "Active silicon integrated nanophotonics: Ferroelectric $BaTiO_3$ devices," Nano Lett. **14**(3), 1419–1425 (2014).

[10]F. Eltes, D. Caimi, F. Fallegger, M. Sousa, E. O'Connor, M. D. Rossell, B. Offrein, J. Fompeyrine, and S. Abel, "Low-loss $BaTiO_3$–Si waveguides for nonlinear integrated photonics," ACS Photonics **3**(9), 1698–1703 (2016).

[11]P. Castera, D. Tulli, A. M. Gutierrez, and P. Sanchis, "Influence of $BaTiO_3$ ferroelectric orientation for electro-optic modulation on silicon," Opt. Express **23**(12), 15332 (2015).

[12]S. Jesse, A. P. Baddorf, and S. V. Kalinin, "Switching spectroscopy piezoresponse force microscopy of ferroelectric materials," Appl. Phys. Lett. **88**(6), 62908 (2006).

[13]C. Thiele, K. Dörr, S. Fähler, L. Schultz, D. C. Meyer, A. A. Levin, and P. Paufler, "Voltage-controlled epitaxial strain in $La_{0.7}Sr_{0.3}MnO_3$/$Pb(Mg_{1/3}Nb_{2/3})O_3$-$PbTiO_3$(001) films," Appl. Phys. Lett. **87**(26), 262502 (2005).

[14]C. Thiele, K. Dörr, O. Bilani, J. Rödel, and L. Schultz, "Influence of strain on the magnetization and magnetoelectric effect in $La_{0.7}A_{0.3}MnO_3$/PMN−PT (001) (A = Sr, Ca)," Phys. Rev. B **75**(5), 54408 (2007).

[15]O. Bilani-Zeneli, A. D. Rata, A. Herklotz, O. Mieth, L. M. Eng, L. Schultz, M. D. Biegalski, H. M. Christen, and K. Dörr, "$SrTiO_3$ on piezoelectric PMN-PT(001) for application of variable strain," J. Appl. Phys. **104**(5), 54108 (2008).

[16]M. Choi, A. B. Posadas, C. A. Rodriguez, A. O'Hara, H. Seinige, A. J. Kellock, M. M. Frank, M. Tsoi, S. Zollner, V. Narayanan *et al.*, "Structural, optical, and electrical properties of strained La-doped $SrTiO_3$ films," J. Appl. Phys. **116**(4), 43705 (2014).

[17]P. Ponath, A. O'Hara, H.-X. Cao, A. B. Posadas, R. Vasudevan, M. B. Okatan, S. Jesse, M. Berg, Z. Li, D. Zhang *et al.*, "Contradictory nature of Co doping in ferroelectric $BaTiO_3$," Phys. Rev. B **94**(20), 205121 (2016).

[18]Q. Wang, J. Wang, and M. J. Kim, "Simple specimen preparation method for in situ heating experiments," Microsc. Microanal. **22**(S3), 132–133 (2016).

[19]A. Herklotz, J. D. Plumhof, A. Rastelli, O. G. Schmidt, L. Schultz, and K. Dörr, "Electrical characterization of PMN–28%PT(001) crystals used as thin-film substrates," J. Appl. Phys. **108**(9), 94101 (2010).

[20]B. Zhi, G. Gao, H. Xu, F. Chen, X. Tan, P. Chen, L. Wang, and W. Wu, "Electric-field-modulated nonvolatile resistance switching in VO_2/PMN-PT(111) heterostructures," ACS Appl. Mater. Interfaces **6**(7), 4603–4608 (2014).

[21]T. Wu, P. Zhao, M. Bao, A. Bur, J. L. Hockel, K. Wong, K. P. Mohanchandra, C. S. Lynch, and G. P. Carman, "Domain engineered switchable strain states in ferroelectric (011) $[Pb(Mg_{1/3}Nb_{2/3})O_3]_{(1-X)}$-$[PbTiO_3]_x$(PMN-PT, x ≈ 0.32) single crystals," J. Appl. Phys. **109**(12), 124101 (2011).